Dynamic Deformation of Soft Particle in Dual-trap Optical Tweezers

Sebastien Rancourt-Grenier[a], Ming-Tsu Wei[b], Jar-Jin Bai, Arthur Chiou[b],
Paul Bareil[a], Pierre-Luc Duval[a] and Yunlong Sheng*[a]

[a]Center of Optics, Photonics and Lasers, Dept. of Physics, University Laval, Quebec Canada;
[b]Institute of Biophotonics Engineering, National Yang-Ming University, Taipei, Taiwan

*sheng@phy.ulaval.ca; phone 1 418 656-2131 3908; fax 1 418 656-2623; fourier.phy.ulaval.ca/~sheng

ABSTRACT

The dual-trap optical tweezers is used for deforming and measuring the elasticity of soft particles suspended in aquatic buffer. In the experiment the trapped particle was the Red Blood Cell (RBC) swollen to a spherical form. The 3D radiation stress distribution was computed by ray tracing, the generalized Lorentz-Mie scattering theory with the T-matrix and the FDTD via the Maxwell stress tensor. The 3D deformation of the cells was then computed with the elastic membrane theory. The calculated deformation can fit to experimental data resulting in cell's elasticity coefficient. The static approach is valid only for small deformation (5-10%). For a large deformation such as that of the RBC, we consider re-distribution of the radiation stress on the morphologically deformed cell. This stress re-distribution in turn induces subsequent deformation of the deformed cell and new stress re-distribution. The recursive process continues until a final equilibrium state is achieved. This iterative computation was implemented with the finite element method using the COMSOL[TM] multi-physics models. The deformation results can fit to the experimental data for cell's deformation up to 20%.

Keywords: Optical tweezers; Optical manipulation; Cell mechanics; Red Blood Cells; Mechanics of Membrane; Elastic deformation; Finite Element methods; Multi-physics.

1. INTRODUCTION

Mechanical properties of the biological cells in vivo determine the behaviour of the cell for the growth, migration and transformation and therefore are equally important as the cell's bio-chemical properties. Optical tweezers are used for manipulating living cells and imposing systematically controlled stress states on the cells to study the constitutive response of the cell membrane and cytoskeleton to physical, chemical, and biological environmental conditions [1-3]. For the suspended cells Guck et al captured and deformed a Red Blood Cell (RBC) in a counter-propagating two-beam optical stretcher for measuring cell's elasticity, whose modification could results from some clinical diseases [3]. The dual trap optical tweezers has been used to apply radiation forces via two beads attached to the cell [4, 5]. In this case the mechanical loading is localized in the regions where the beads are bound to the cell. The dual or triple-traps have been also applied directly to the cells without attached beads [6-8].

In this paper, we use a dual-trap optical tweezers to trap and deform a RBC swollen to spherical shape with experimental results fit to a quantitative analysis of the 3D radiation stress distribution and the corresponding 3D deformation. All the previous works [3, 8-10] considered only the static deformation, that is to compute first the radiation stress on the trapped cell and then the consequent cell's deformation using linear elastic theory of membrane. This analysis is valid only for small deformation of about 5-10%. However, the RBCs usually undergo much larger deformation. In the case of large deformation of the cell, the re-distribution of the radiation stress on the deformed cell should be considered and the deformed cell will be further deformed under the redistributed stress. In this paper we consider this dynamic regime of the deformation and compute the stress redistributions and the subsequent deformations in a recursive manner until a finale equilibrium state is reached. Fit the theoretical prediction to the experimental data results in the elasticity of the human RBC membrane when the cell's deformation is up to more than 20%.

2. DUAL TRAP OPTICAL TWEEZERS

A schematic diagram of the dual-trap optical tweezers setup is illustrated in Fig. 1. A linearly polarized laser beam (λ = 1064 nm, 1W, Nd: YVO$_4$ cw laser) was split into two via a polarizing beam splitter (PBS) and recombined by a second polarizing beam splitter (PBS) to form two parallel trapping beams focused by an oil immersion microscope objective (NA=1.25, 100X) in the interior of the captured RBC, which was swollen to spherical and suspended in saline (150 mOsm) buffer solution. The optical powers of the two beams can be adjusted by rotating the half-wave (HW) plate. One of the laser beams can be laterally shifted by a motorized translational stage (MS).
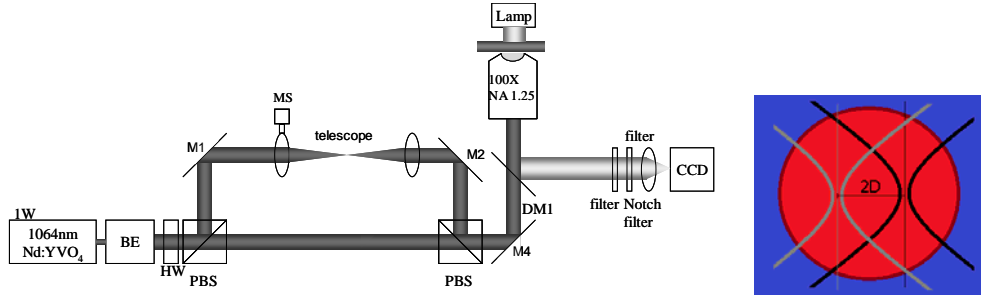
Fig.1. A schematic diagram of the experimental setup.

The distance D between the focal spots was increased from 0 μm to 6.34 μm in 6 discrete steps. As the cell's reaction to the external load is typically slow, in the experiments we increased the beam separation D stepwise and always allowed enough time for the cell to reach equilibrium before the next increase of D. Wide-field images of the trapped RBC along the trapping beam axis were captured by a CCD camera with a pre-calibrated length-scale, as shown in Fig. 2a and 2b, for the RBCs without drug treatment and with the 1mM N-ethylmaleimide (NEM) treatment for 30 minutes for the different separations D. In each step we measured the length of the major axis of the RBC along the direction of the beam separation.

(a)

(b)
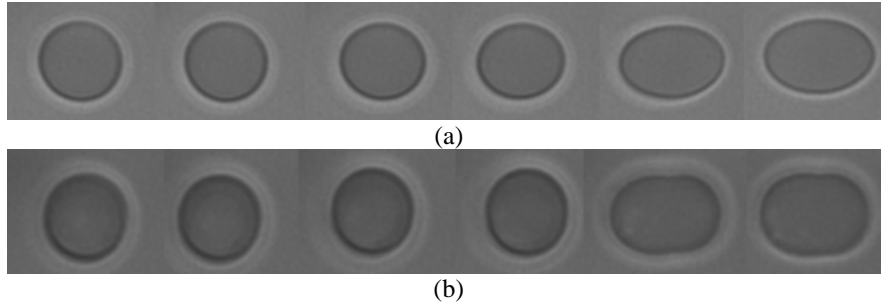
Fig.2. Images of a trapped and stretched RBC: (a) without drug treatment; (b) with 1mM N-ethylmaleimide (NEM) treatment for 30 minutes as a function of the dual beam separation D = 0, 1.27, 2.54, 3.80, 5.07 and 6.34 μm (from left to right);
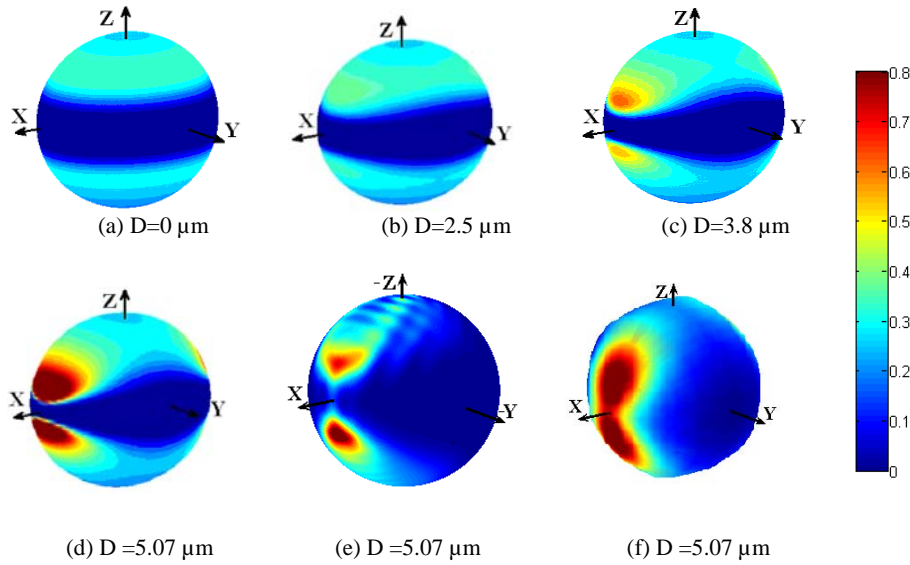
3. 3D STRESS DISTRIBUTION

The radiation stress on the RBC surface associated with the two highly focused trapping beams focused at ($x = \pm D/2$, $y = z = 0$) can be computed with the geometric optics ray-tracing, the T-matrix approach based on the generalized Lorentz-Mie diffusion theory (GLMT) [11]. Ideally, the stress can be computed by solving the electromagnetic field using the Finite Difference in Time Domain method such as Optiwace^{TM} and/or the finite element methods, such as the RF module Comsol Multiphysics^{TM} via the Maxwell stress tensor. However, the highly focused Gaussian beams with NA=1.25 need to be properly modeled in these software.

The radiation stress is computed by the photon momentum conservation. According to the Minkowski model the photon momentum is proportional to the index of refraction of the material n, P = nE/c with the beam energy E and speed of light c, so that

$$\vec{\sigma} = \frac{1}{c}\frac{E_i}{A\Delta t}n_1\left(\vec{a}_i - \left(nT\vec{a}_t + R\vec{a}_r\right)\right) \qquad (1)$$

where $\vec{a}_i$, $\vec{a}_t$ and $\vec{a}_r$ are the unit vectors of the incident, transmitted, and reflected beam, respectively, A is the area covered by the beam, P is the beam power and $n = n_2/n_1$. When $n_1=1.335$ of the medium surrounding the cell, and $n_2=1.378$ of the cytosol inside the cell, T and R are the Fresnel transmission and reflection coefficient respectively. In the case of the RBC, the R of the cell/buffer interface is very small for a large range of the incident angle, about 99% light is transmitted, so that the light entering to the cell gains the momentum due to the higher refraction index inside, the radiation stress is opposite to the light propagation, and the light exiting the cell losses momentum, the radiation stress is along the light propagation. In both cases the direction of $\vec{\sigma}$ is outward from the cell.

The results are shown in Fig. 3. When the beam separation $D=0$, the stress distribution is revolutionary symmetric with respect to the z-axis, and there is a crown-shaped region around the equator of the sphere in the x-y plane, on which only few or no optical rays incident, so that the stress is low or equal to zero, as shown in Fig. 3a. The width of this region depends on the numerical aperture of the trapping beam and the size of the cell. When the beam focus is shifted along the x-axis, the stress distribution remains practically unchanged in the range of $D < 2$ μm for a RBC radius of about 7 μm, as shown in Fig. 3b. In the view of projection along the z axis the cell is not elongated along the $\pm x$ axis. This is in agreement with the experimental observation [8] and with the photographs shown in Fig. 2a and 2b for D=1,27–2,54 μm. When the beam shift D continues to increase the stress is concentrated gradually towards the x-y plane and towards the $\pm x$ directions with the magnitude of the stress peaks increasing significantly, as shown in Fig. 3c-3d.

(a) D=0 μm	(b) D=2.5 μm	(c) D=3.8 μm
(d) D =5.07 μm	(e) D =5.07 μm	(f) D =5.07 μm

Fig. 3. 3D stress distribution (N/m^2) on spherical surface of a cell in suspension in the dual-beam optical tweezers with D as separation distance of two trapping beams, computed with ray-tracing (a)–(d), with T-matrix (e) and with FDTD (f). The trapping beams of NA=1.25, power P=89mW are along the +z-axis. The cell radius ρ= 3.86 μm, the refractive index in buffer n$_1$=1.335 and inside the cell n$_2$=1.378

The T-matrix and the FDTD produced similar results as that did the ray-tracing, for the beam separation $D = 5.07$ μm, as shown in Fig. 1e and 1f. Their differences were mostly due to the different models for the highly focused beam. The ray optics approach is valid approximately as the RBC diameter $2\rho \sim 7\ \mu m$ is larger than the wavelength λ=1.06 μm, [1,3, 8, 9]. In the FDTD, a paraxial Gaussian beam model was used because of the limitation in the interface of the Optiwace^{TM} software. This is a rough approximation for the highly focused beam. On the other hand, in the T-matrix method the trapping beam was decomposed into the vector spherical wave-function (VCWF) basis satisfying the vector Helmholtz equation with the expansion coefficients computed by point matching method to match by matching the far field distribution of the VSWF expansion to the the TEM$_{00}$ (or LG$_{00}$) laser beam in far field [12].

4 STATIC DEFORMATION

In the "liquid-interior model" [14,15], the RBC consists of a thin membrane containing incompressible fluid (cytosol). The RBC memembrane consisting of a phospholipid bilayer, a spectrin filament network and transmembrane proteines can be treated as a hyperelastic effective continuum layer. The ratio between the thickness h of the memembrane and the cell radius ρ is $h/\rho \sim 1\%$ [3], so that the RBC's deformation under the radiation stres can be computed using the classical elastic membrane theory, in which the membrane is considered to have finite flexural stiffness to resist in-plane tensile or compressive forces, but cannot support off-plane bending and twisting forces.

The RBCs were initially swollen from physiological biconcave shape to a spherical shape by the osmotic pressure. Once captured by the dual trapping beams, the RBC received an additional radiation stress as external load and was deformed to a new state of equilibrium in which the external load is balanced by the membrane internal force. For the spherical RBC the equilibrium equations are given by [16].

$$\frac{\partial N_\theta}{\partial \theta} + \sin\varphi \frac{\partial S}{\partial \varphi} + 2S\cos\varphi = 0 \tag{2.1}$$

$$\frac{\partial N_\varphi}{\partial \varphi}\sin\varphi + (N_\varphi - N_\theta)\cos\varphi + \frac{\partial S}{\partial \theta} = 0 \tag{2.2}$$

$$N_\theta + N_\varphi + \rho\sigma_r = 0 \tag{2.3}$$

where N_ϕ and N_θ are the membrane forces per unit length, applied normally to the boundaries of a differential membrane element in the zenith and the azimuth directions, respectively, and S is the in-plane shear force per unit length, tangential to the boundaries of the element. One can solve N_ϕ, N_θ and S by Eqs. (2.1)-(2.3), and then associate the stresses to the local strains prescribed by Hooke's law in the limit of the linear elasticity. Finally, the deformation of the cell is described as displacement vectors of the material points on the membrane and can be solved from the local strain by the constitutive equations, which are for the spherical membrane

$$\frac{\partial \upsilon}{\partial \varphi} - \upsilon\cot\varphi - \frac{1}{\sin\varphi}\frac{\partial u}{\partial \theta} = R\left(\frac{N_\varphi - vN_\theta}{Eh} - \frac{N_\theta - vN_\varphi}{Eh}\right) \tag{3.1}$$

$$\frac{1}{\sin\varphi}\frac{\partial \upsilon}{\partial \theta} + \frac{\partial u}{\partial \varphi} - u\cot\varphi = \frac{RS}{Gh} \tag{3.2}$$

$$w = \frac{\partial \upsilon}{\partial \varphi} - \frac{R}{Eh}(N_\varphi - vN_\theta) \tag{3.3}$$

where (u,υ,w) are the displacement in the directions of the curvilinear coordinate system (U,V,W) centered at the differential membrane element, with the W-axis directed inward to the origin of the sphere and (U, V) tangential to the zenith and the azimuth directions, φ and θ, and E is the modulus of elasticity and v is the Poisson coefficient representing the volume change of the membrane due to the deformation. For small deformation the membrane is isotropic and $v=0.5$ approximately.

In the dual-beam optical tweezers the external load $\sigma_r=\sigma_r(\varphi,\theta)$ is not revolutionally symmetric around the z-axis due to the lateral shift of the two beams, as shown in Fig. 3. In this case we can still solve the equilibrium and the constitutive equations analytically by using the Fourier expansions of the external load $\sigma_r=\sigma_r(\varphi,\theta)$ and all other unknown functions in Eqs. (2) and (3) with respect to the azimuth angle θ. The mathematical detail is given in Ref. [17,18]. Figure 4 shows the static deformation for the beam focus separation D = 0, 1.26, 2.54, 3.8, 5.08 and 6.34 μm, respectively. This prediction of cell's deformation can fit to experimental measurement for small beam separations $D<4$μm. For larger D, higher stress and higher deformation, the theoretical prediction of the static deformation is clearly higher than the experimental observation.
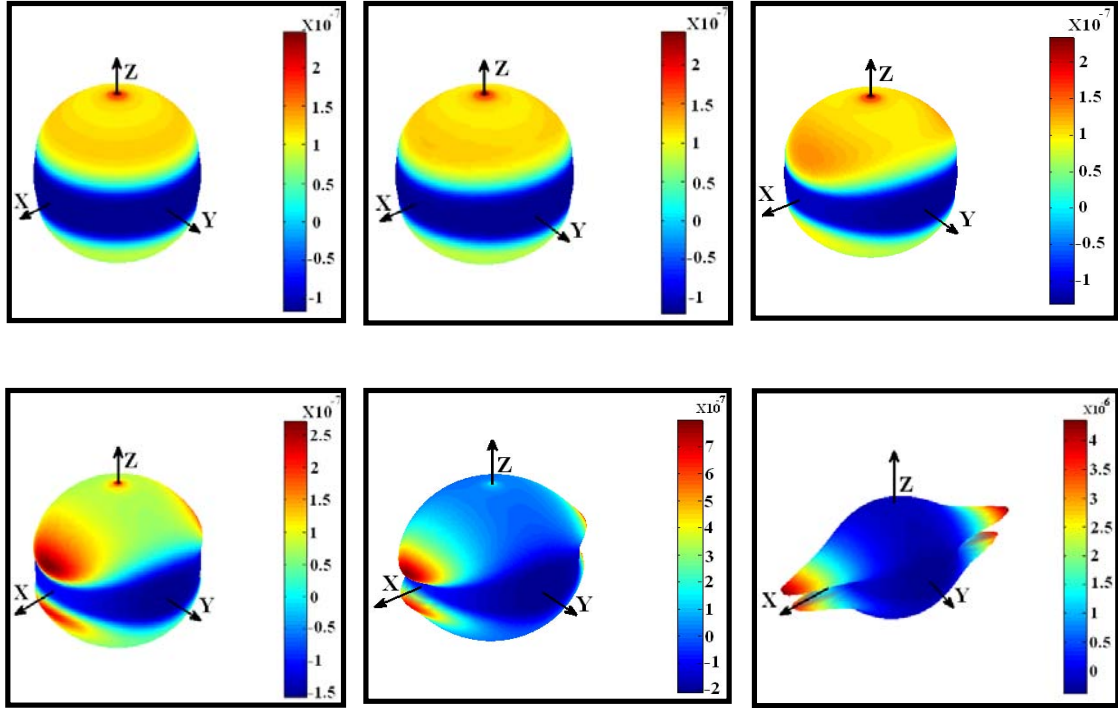
Fig. 4. Deformation of a spherical RBC in suspension in the dual-beam optical tweezers with the separation distance of two trapping beams as: First raw (from left to right) : D = 0, 1.26, 2.54 μm; Second raw (from left to right) D = 3.8, 5.08 and 6.34 μm, computed with Eqs. (2) and (3) component–by-component of the Fourier expansion with respect to azimuth angle [17,18].

5. DYNAMIC DEFORMATION

When the cell's deformation is significant in the dual-trap optical tweezers, the radiation stress re-distribution on the deformed cell's surface must be considered. Furthermore, the stress re-distribution will lead to cell's re-deformation, which in its turn will lead to new re-distribution of the stress. The process continues until a final equilibrium state is reached for a given field of the dual optical trapping beams. However, for the deformed RBC the equilibrium and the constitutive equations are no longer as simple as Eqs. (2) and (3). Their analytical solutions would be more difficult. The finite element solution in Comsol[TM] structured mechanics module was then used. To compute the stress distribution we embedded our Matlab[TM] codes for the ray optics approach to the Comsol[TM] modules. We input to Comsol[TM] structural mechanics module the radius ρ, the membrane thickness h, a test value of the elasticity coefficient E of the RBC membrane and the beam separation value D, and selected a uniform deformable moving mesh on the cell surface.

In the optical tweezers the cell is trapped to an equilibrium position where the net force on the cell is equal to zero. In the equilibrium position, the cell's center will not remain in the focal plane $z = 0$, but is usually shifted in the direction of the laser beam propagation. However, we ignored this slight offset in the calculation of the stress and the deformation, for the sake of simplicity, so that in our model the cell was fixed with its center at the origin of the in the coordinate system, but the net radiation force applied to the cell is not zero. We had to set six constraints that the 6 poles of intersection of the cell surface with the x, y and z axes can move only along the x, y and z axis respectively for preventing the cell from shift in the space. This shift was not of interest when computing the cell's deformation.

We launched the stationary solution solver in the Comsol[TM]. The stress distribution was first computed by our Matlab[TM] codes, and then the cell's deformation under the stress distribution was computed by a linear solver SPOOLES. Once SPOOLES completed its execution, the cell was deformed along with the moving mesh, so that the stresses on the deformed mesh nodes were re-computed using the embedded Matlab[TM] codes for ray-tracing. Then, the SPOOLES was launched again to compute the deformation under the new stress distribution of the deformed mesh nodes. The iterative

process continued until a convergence of the solution was finally reached after 4-5 iterations, and the deformed cell reached a final equilibrium state. We found that the cell's deformation computed in the first iteration of the linear solver SPOOLES with the stress distribution on the initially spherical cell is identical to the static deformation computed by the analytical method shown in Fig. 4. This agreement validates our Comsol[TM] solution.
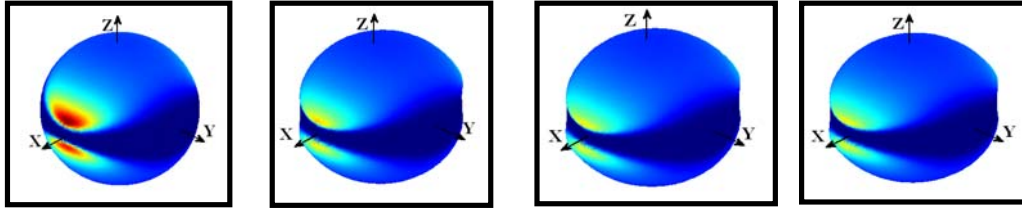
Fig. 5 Stress distribution on an initially spherical cell with radius ρ=3.86 μm and beam separation D = 5.07 μm as the cell is deformed gradually from left to right. Computed in iterations of COMSOL[TM] modules.

Figure 5 shows the stress redistribution on the cell which was initially spherical but gradually deformed in the iterative computations with the beam separation $D = 2.54$ μm. We see in the figure that the peaks of the redistributed stress became wider and the peak values decreased as the cell was deformed progressively. This is fully understandable as the sections of the membrane, in which the most stress was concentrated went away from the laser beam focus with the elongation of the sphere.
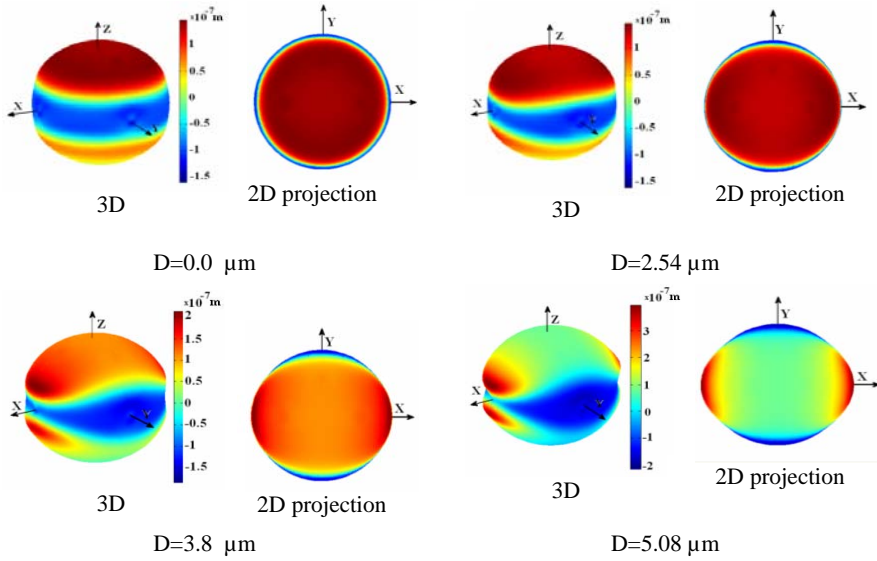
Fig. 6. 3D deformed shape and its 2D projection along the z-axis of a spherical RBC in the dual-trap optical tweezers computed in the dynamic regime. Separation of the two beams along $\pm x$ directions D; Initial spherical cell radius ρ= 3.658 μm, refractive index n_2=1.378 and that in buffer n_1=1.335, Eh=23.77 μN/m. Power of 89 mW for each beam. The colors encode the radial displacements of the membrane, which are positive (outward from the cell) or negative (inward to the cell)

As a result, the final cell's deformation in the dynamic regime is quit different from that computed in the static regime without considering the re-distribution of the stress. The dynamic regime is closer to the physical reality for larger deformations. Figure 6 shows the computed final deformation of a spherical RBC in the dual beam optical tweezers as a function of the beam separation distance D, in the dynamic deformation regime with the consideration of the stress redistribution on the deformed cell. The projections of the 3D shapes of the deformed cells along the z-axis to the x-y plane are the ellipses elongated in the $\pm x$ directions as observed in the experiments, and shown in Fig. 2a and 2b. The cell's deformation along the z-axis was not readily observable in the experiments.

The cell's deformation was described by the length of the major axis of the projection of the deformed cell shapes along the z-axis to the x-y plane. We fit the theoretical predicted cell's deformation to the experimental data. The fitting parameters were the product of the membrane elasticity and the membrane thickness Eh and the cell's initial radius ρ. As ρ can vary in experiments among the group of 30 samples, we took ρ as a fitting parameter. We found Eh=15.99 (μN/m) and ρ=3.554μm for the normal RBC's and Eh=24.39 (μN/m) and ρ=3.697μm for the RBCs with the drug treatment. The corresponding shear modulus are $Gh = Eh/2(1+v) = 5.33$ and 8.13 (μN/m), respectively.

(a)   (b)
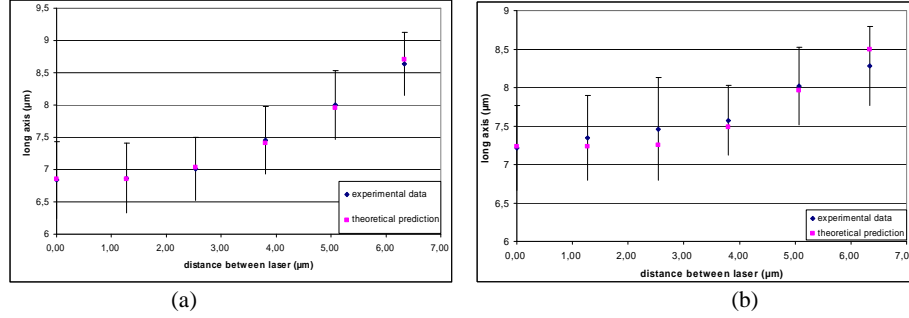
Fig.7. Theoretical prediction fit to experimental data for the length of the major axis as a function of beam separation D = 0, 1.27, 2.54, 3.80, 5.07 and 6.34 μm; (a) without drug treatment, Eh=15.99 (μN/m) ρ=3.554 μm; (b) with treatment of 1mM N-ethylmaleimide (NEM) for 30 minutes, Eh=24.39 (μN/m) ρ=3.697 μm. Error bars show the root-mean-square standard deviation of the measurements over 30 samples under the same condition.

Our fitting is valid for more than 20% of deformation, measured as a ratio of the elongation of the long axis length to the cell's initial diameter. A RBC in suspension can usually restore its initial shape after such a large deformation [15]. When the RBC is elongated by 20%, its membrane parts are not necessarily stretched or compressed by 20%. This is similar to a balloon in air, which can undergo a large deformation keeping in a constant volume before explosion. The RBC shape deformation can be caused by certain deformations of the membrane parts along with certain simple displacements of the membrane elements, so that under 20% elongation the RBC is still in linear elastic deformation regime.

6 CONCLUSION

We have implemented calculation of the 3D dynamic deformation of the red blood cell with the finite element method and Comsol Multiphycis[TM] modules along with the embedded ray-tracing codes to compute the stress distribution on the deformed cell. Our tool thus combines the geometrical optics and the structure mechanics into the single calculation. This allows computing the stress re-distribution and cell's re-deformation in the iterations. The theoretical predictions fit to the experimental data permitting differentiating the red blood cells with and without the drug treatment and obtaining the cell membrane's elasticity coefficients. This approach allows us to evaluate large deformation of RBCs in the dual-trap optical tweezers up to 20%. Instead of 5-10% in the previous implementations.

Ideally, we should use the RF electromagnetic Comsol Multiphycis[TM] module along the Structural mechanics module to compute the interaction between the field of the laser trapping beams and the deformable trapped particles, which could be not spherical but in their natural forms, such as biconcave form of the red blood cells. We should be able to treat the entire trapping problem with the Comsol Multiphycis[TM] modules and let particle floating in the space to be stabilized finally in the equilibrium position. To achieve this objective we need the RF module able to model the highly focused laser beam and permit a large space domain in the calculation.

REFERENCES

[1] Ashkin and Dziedzic, J. M., "Optical trapping and manipulation of single cell using infrared laser beams," Nature **330**, 769-771 (1987).

[2] Block, S. M., "Making light work with optical tweezers". Nature 360, 493-495 (1992)

[3] Guck, J. Ananthakrishnan, R., Mahmood, H., Moon, J. T., Cunninghan, C. C., and Kas, J., "The optical stretcher: a novel laser tool to micromanipulate cells," Biophys. J. **81**, 767-784 (2001).

[4] Dao, M., Lim, C.T., Suresh, S., "Mechanics of the human red blood cell deformed by optical tweezers", J. Mechanics Physics of Solids, 51 2259 – 2280 (2003)

[5] He´non, S., Lenormand, G., Richert, A. and Gallet, F., "A new determination of the shear modulus of the human erythrocyte membrane using optical tweezers," Biophys. J. **76**, 1145-1151 (1999).

[6] Bronkhorst, P. J. H., Streekstra, G. J., Grimbergen, J., Nijhof, E. J., Sixma, J. J., and Brakenhoff, "A new method to study shape recovery of red blood cells using multiple optical trapping," Biophys. J. **69**, 1666-1673 (1995).

[7] Lee, W. G., Bang, H., Park, J., Chung, S., Cho, K., Chung, C., Han, D. C. and Chang, J. K., "Combined microchannel-type erythrocyte deformability test with optical tweezers," *Proc. of SPIE.* **6088**, 608813-1-12, (2006).

[8] Liao, G. B., Bareil, P. B., Sheng Y. and Chiou, A., "One-dimensional jumping optical tweezers for optical stretching of bi-concave human red blood cells" Opt. Express **16**, 1996-2004 (2008)

[9] Bareil, P.B., Sheng, Y. and Chiou, A. "Local stress distribution on the surface of a spherical cell in an optical stretcher," Opt. Express **14**, 12503-12509 (2006).

[10] Guck, J., Ananthakrishnan, R., Mahmood, H., Moon, T. J., Cunningham, C.C., and Käs, J., "The optical stretcher: a novel laser tool to micromanipulate cells," Biophys. J. **81,** 767-784 (2001).

[11] Nieminen, T. A., Loke, V. L. Y., Stilgoe, A. B., Knoner, G., Branczyk, A. M., Heckenberg, N. R. and Dunlop, H. R., "Optical tweezers computational toolbox", J. Opt. A Pure Appl. Opt, **9**, s196-s203 (2007)

[12] Nieminen, T.A., Rubinsztein-Dunlop, H., Heckenberg, N.R., Multipole expansion of strongly focussed laser beams, Journal of Quantitative Spectroscopy & Radiative Transfer 79–80, 1005–1017 (2003)

[13] Mansuripur, M., "Electromagnetic stress tensor in ponderable media", Optics Express vo. 16, No. 8, 5193-5198(2008)

[14] Xu, F., Lock, J. A., Gouesbet, G. and Tropea, C., "Optical stress on the surface of a particle: homogeneous sphere", Phy. Rev. A, 79, 053808 (2009)

[15] Fung, Y. C., "Theoretical considerations on the elasticity of red cells and small blood vessels," Federation Proceedings 25, 1761-1769 (1966)

[16] Bareil, P. B., Sheng, Y., Chen, Y. Q. and Chiou, A., "Calculation of spherical red blood cell deformation in a dual beam optical stretcher", Optics Express, vol. 15 No. 24, 16029-16034 (2007).

[17] Rancourt-Grenier, S., Wei, M., Bai, J., Chiou, A., Bareil, P., Duval P. and Sheng, Y., "Dynamic deformation of red blood cell in Dual-trap Optical Tweezers", Optics Express, vol. 18, No. 10, 10462-10472 (2010).

[18] Ventsel E. and Krauthammer, T. [Thin plate and shells], Marcel Dekket, New York, (2001).